THE JOURNAL OF PHYSICAL CHEMISTRY C

Article

pubs.acs.org/JPCC

Molecular Electronic Effects on the Thermal Grafting of Aryl Iodides to TiO_2 Surfaces

Caroline R. English and Robert J. Hamers*

Department of Chemistry, University of Wisconsin—Madison, 1101 University Avenue, Madison, Wisconsin 53706, United States

Supporting Information

ABSTRACT: Recent studies have shown that aromatic iodides can readily graft to hydroxylated surfaces of TiO_2 and other metal oxides, forming a convenient route to molecular functionalization of metal oxides. While these reactions appear similar to the Williamson ether synthesis of organic chemistry, the S_N2 mechanism typically invoked in solution phase reactions is less accessible on surfaces, and the mechanism of the surface reactions is poorly understood. We have undertaken a combined experimental and computational study in an effort to understand how the molecular electronic structure impacts the surface reactivity. Computational studies of reaction enthalpies were compared were used to generate Hammett plots that were then compared to experimental measurements of surface grafting rate for molecules with different substituent groups. Our results show that there is poor correlation between Hammett parameters and surface reactivity. Additional experiments were conducted to evaluate the impact of molecular hydrophobic character on reaction rate. Our results suggest that radical reactions or other pathways are likely responsible for controlling reactivity of aromatic halides with TiO_2 surfaces.

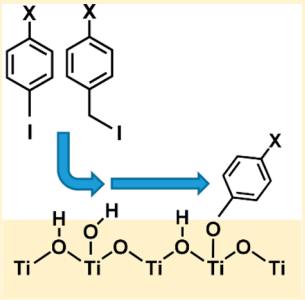

INTRODUCTION

The functionalization of metal oxides using conjugated molecules is of interest for emerging solar energy harvesting applications.[1−4] For these new applications, functionalizing metal oxides with photodyes[1−7] and photocatalysts[4,8−10] integrates the mechanical and electrical properties of the oxide with the electronic tunability of the arene. This sensitization forms a new molecule−metal oxide interface in these devices that affects overall device properties. As a consequence, there has been sustained interest in studying and manipulating the molecule−metal oxide interface.[4−6,11−24]

Research toward molecular engineering of molecular sensitizers and photocatalysts consists primarily of studying the impact of anchor groups[14−19,25,26] and molecular structure on solar conversion performance.[3,19,20,25,27−38] One way to tune the molecular electronic structure is through incorporating electron-withdrawing and electron-donating moieties on the dye.[3,38] However, there are cases where through electrostatic effects such molecular functional groups either activate or deactivate a molecule from participating in a reaction. For example, functional groups affect molecule reactivity during electrophilic and nucleophilic aromatic substitution in organic chemistry.[39−43] These reactions are relevant to hybrid solar cells because aromaticity controls the light absorption properties of photoresponsive molecules. While much effort has been exerted toward engineering new photoresponsive molecules[27−31,44−47] in order to improve device performance, less effort has been shown toward understanding how altering the functional groups present will affect the rate of molecular adsorption and thermodynamic stability of the resulting molecule−surface adducts.

We have shown that iodo−aryl and −benzyl compounds will react with the Ti−OH groups on TiO_2 surfaces under mild conditions, presumably with formation of direct Ti−O−molecule linkages.[13] The grafting of the iodo−aryl species is especially noteworthy because organic alcohols are unreactive toward aryl iodides in organic chemistry, while the analogous reaction with titanol (Ti−OH) groups is facile. The formation of direct molecule−TiO_2 linkages with no intervening atoms is important because such a linkage can provide a more direct pathway for electronic communication between the π-electron system of the molecular aromatic ring and the conduction band of the TiO_2 surface. Such a direct linkage could lead to increased electron transfer efficiency across the molecule−metal oxide interface in photovoltaic devices.[5,20,25,48−50] Other benefits of this new functionalization method include increased water stability over carboxylate linkages[13] and the removal of the acidic COOH moieties currently used for anchoring the molecule to the semiconductor surface. These moieties can etch away acid-sensitive metal oxides like ZnO that are also of interest for solar cell applications.[19,51]

Here, we report an investigation of how electron-withdrawing and electron-donating substituent groups influence the reactivity and stability of arene−TiO_2 interfaces. By integrating experimental and computational analyses, our results provide new insights into the factors that influence the formation and stability of the resulting arene−TiO_2 interfaces.

Received: August 27, 2015
Revised: November 1, 2015
Published: November 11, 2015

DOI: 10.1021/acs.jpcc.5b08333
J. Phys. Chem. C 2015, 119, 27972−27981

EXPERIMENTAL SECTION

Preparation of TiO_2 Nanocrystalline Thin Films. Nanocrystalline TiO_2 films were made using commercially available paste (Ti-Nanoxide T/SP, 15−20 nm particle size, Solaronix, Switzerland). The TiO_2 paste was screen-printed onto substrates consisting of 20 nm of Ti evaporated onto single-crystalline, high-resistivity, float-zone-refined Si(001). The use of a thin Ti layer improved the adhesion to the substrate without introducing interference effects in Fourier transform infrared (FTIR) spectroscopy measurements. After screen-printing, the films were first dried at 110 °C prior to annealing at 500 °C. For the annealing process, the temperature was ramped to 500 °C over 30 min and then held at temperature for 15 min. Before use, the TiO_2 films received a NaOH (pH ∼ 11) base pretreatment for at least 20 min followed by rinsing with isopropanol a minimum of three times. After each isopropanol rinse, the films were dried with N_2.

Mass Spectrometry TiO_2-Coated Sample Vial Preparation. We used anatase TiO_2 nanoparticles synthesized through scaling up a previously published procedure[52] for mass spectrometry studies. The anatase TiO_2 nanoparticles were suspended in ethanol and crashed out of suspension using diethyl ether and centrifuging for 10−20 min at 5000 rpm. Once the nanoparticles were isolated, they were transferred to mass spectrometry reaction vials and dried by heating the vials at 120 °C. All reaction vial walls were coated in the TiO_2 nanoparticle paste prior to heating in order to cover the glass. The TiO_2-coated reaction vials were placed in a humid environment in order to replace the water adsorbed on the TiO_2 surfaces that was lost upon heating.

TiO_2 Thin Film Functionalization. TiO_2 thin films were submersed in either 1-iodo-4-(trifluoromethyl)benzene (I−C_6H_4−CF_3), 1-fluoro-4-iodobenzene (I−C_6H_4−F), iodobenzene (I−C_6H_5), 1-iodo-4-methylbenzene (I−C_6H_4−CH_3), or 1-iodo-4-methoxybenzene (I−C_6H_4−OCH_3) and placed in a 65 °C oven. Reaction times ranged from 5 min to 6 h. Before reaction, FTIR was used to check that minimal C−H stretching was observed. A piece of the titanium-coated silicon substrates used during TiO_2 thin film deposition was used as a FTIR reference (background) sample. Thin films were blown with N_2 until the C−H stretching region stayed consistent based on FTIR spectra. Then, FTIR spectra were collected of each thin film prior to the thermal grafting reaction.

After reaction, the samples were rinsed at least three times with solvent and dried with N_2 after each rinse to remove any excess adsorbed materials. Isopropanol was used for rinsing in all cases except for I−C_6H_4−OCH_3 runs; for reactions involving I−C_6H_4−OCH_3, acetone was used in place of isopropanol for rinsing samples after reaction. This change in solvent was due to I−C_6H_4−OCH_3 being insoluble in isopropanol.

Fourier Transform Infrared (FTIR) Spectroscopy. Single-bounce reflection Fourier transform infrared (FTIR) spectra were obtained using a Bruker Vertex 70 FTIR spectrometer using a liquid nitrogen-cooled HgCdTe detector. The spectrometer was equipped with a Veemax II variable-angle single-bounce reflection accessory. Single-bounce reflectance measurements were taken using p-polarized light at a 50° angle of incidence from the surface normal and a resolution of 4 cm^{-1}. A piece of float-zone-refined Si(001) with 20 nm of titanium evaporated on its surface was used as a reference (background) sample after receiving the same heat treatment as the TiO_2 thin films. Absorbance spectra measured before thermal grafting were subtracted from spectra measured after thermal grafting in order to obtain difference spectra. The difference spectra helped isolate absorbance changes occurring upon surface functionalization. Undulating backgrounds were flattened by identifying regions across the entire spectrum with no sharp features, fitting these regions to a sixth-degree polynomial function, and then subtracting the polynomial from the raw data.

Mass Spectrometry. The thermal grafting reaction was performed inside TiO_2-coated glass vials while the loss of water as the reaction progresses was determined *in situ* using mass spectrometry. Anatase TiO_2 nanoparticles were crashed out of solution and used to coat the inside of glass vials used as reaction vessels for mass spectrometry analysis. The TiO_2 slurry was spread along the inside of the vials using the side of a glass pipet, and then the vials were gently heated to 120 °C in order to dry the TiO_2 slurry inside the glass vials. The vials were stored in a humid environment until experiments were performed to ensure the presence of water on the TiO_2 surfaces.

The temperature of the reaction vessels was controlled using a programmable temperature controller (PTC 10, Stanford Research Systems). Argon gas passed over the reaction vessel, and the sample head space was continuously sampled using a universal gas analyzer (UGA100, Stanford Research Systems). The reaction vessel was held at a constant 65 °C for 3 h, mirroring reaction conditions used in FTIR experiments. Mass spectra were continuously collected upon reaching the set temperature. Each mass spectra consisted of five scans over a range of 17−19 amu.

Nuclear Magnetic Resonance (NMR) Spectroscopy. ^1H nuclear magnetic resonance spectroscopy was performed using a Bruker Avance III 500 instrument equipped with a SmartProbe. Quantitative NMR experiments were performed at 65 °C in D_2O to determine the water solubility of the aromatic molecules used in TiO_2 functionalization. Sodium-3-(trimethylsilyl)-1-propanesulfonic acid was used as an internal standard for peak shifts and peak integrations. NMR samples were prepared by mixing 0.5−0.6 mM solutions of known internal standard concentrations in D_2O with excess amounts of the neat aromatic compounds and then placing this mixture into a 65 °C oven for at least 1 h. After heating the mixtures, some of the D_2O layer was carefully pipetted out of the sample vial and into NMR tubes. The NMR samples were stored in the oven until ready to be loaded into the NMR sample queue.

Vienna *ab Initio* Simulation Package (VASP). Density functional theory calculations were performed using the Vienna Ab-initio Simulation Package (VASP) version 4.6.[53−56] Projector-augmented plane waves[57,58] combined with the PBE density functional[59,60] were used for all calculations. 2 × 2 slab models of the anatase TiO_2(001) surface were used to model the functionalization of the TiO_2 surface. The minority (001) surface was chosen due to the increased dissociative adsorption and charge separation shown by the (001) face versus the thermodynamically favorable (101) face.[61−67] The dissociative adsorption results in two distinct types of surface OH groups: one, referred to as a "terminal" −OH group, arises from adsorption of OH onto an under-coordinated Ti site. The second, referred to as a "bridging" −OH group, arises from protonation of an exposed O atom that is bonded to multiple Ti atoms.[13,68,69] These two types of OH groups are expected to act as the reactive surface sites and form Ti−O−C ether-like

DOI: 10.1021/acs.jpcc.5b08333
J. Phys. Chem. C 2015, 119, 27972−27981

bonds with the molecules. The *z*-axis height was set to 50 Å for all calculations to ensure at least 14 Å of vacuum space between functionalized slabs.

Γ-point geometry optimizations were performed using Gaussian smearing with a 0.05 eV smearing width. SCF convergence was set to 10^{-6} eV. The conjugate gradient algorithm was used for ionic updating, and the ionic movement stopping criterion was set to 0.01 eV/Å.

Static self-consistent calculations were performed after geometry optimizations. For these calculations, the tetrahedron method with Blöchl corrections was used with a 3 × 3 × 1 Γ-centered Monkhorst Pack[70] k-point mesh. The SCF convergence criterion was adjusted to 10^{-7}eV, and the precision for the calculations was set to "accurate".

Natural Bond Orbital (NBO) Analysis. Natural bond orbital (NBO) analysis was performed using the geometry-optimized VASP outputs.[71] The optimized plane waves were projected into the 3-21G basis set for all atoms. For this process, symmetry was turned "off", and a static self-consistent calculation was performed in order to obtain plane waves compatible with the basis set projection.

RESULTS

Computational Comparison of Reactivity of Terminal vs Bridging Ti−OH Groups. The periodicity imposed on the calculations through the use of plane waves in VASP leads to each TiO_2 slab having both a top and bottom surface available for reaction. Therefore, in calculating the changes in enthalpy for each reaction, we first functionalized both slab surfaces and then divided the resulting energy in half to obtain the adsorption enthalpy per molecule. Unless otherwise stated, all adsorption enthalpies reported in this work are for the reaction of one molecule with the surface of TiO_2.

In order to calculate enthalpies of adsorption, we performed calculations and obtained enthalphies of formation for all reactants and products in the thermal grafting reaction. We then subtracted the enthalpies of formation of the reactants from those of the products. We assumed all reactions produced HI in molecular form as a reaction byproduct in order to balance the chemical equations. The assumption that HI is the reaction byproduct introduces the same systematic error into all reaction enthalpies, so our analysis is unaffected by this assumption.

We looked at the difference in enthalpy change when I−C_6H_4−CF_3 and 1-iodomethyl-4-(trifluoromethyl)benzene (I−CH_2−C_6H_4−CF_3) react with either the terminal or bridging Ti−OH sites present on the TiO_2 surface. Comparing I−C_6H_4−CF_3 to I−CH_2−C_6H_4−CF_3 allows us to determine the effects a CH_2 spacer group has on thermodynamic bond stability. Figure 1 shows the four possible combinations that were compared in order to determine enthalpy changes associated with either alternating the surface TiOH site or the molecule involved in the reaction. Figure 1a shows the reaction of I−C_6H_4−CF_3 with the terminal TiOH group while Figure 1b shows the reaction of I−C_6H_4−CF_3 with the bridging TiOH group. The terminal and bridging TiOH groups are also shown reacting with I−CH_2−C_6H_4−CF_3 in Figures 1c and 1d, respectively.

Figure 2 plots the predicted changes in enthalpy for each reaction shown in Figure 1. We have labeled the data points with the reactants involved in each system. All enthalpy changes in Figure 2 are referenced to the enthalpy change for the terminal TiOH reacting with I−C_6H_4−CF_3 (the ΔH for this

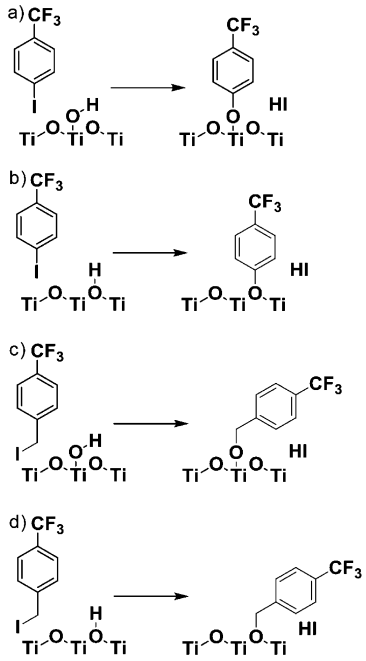

Figure 1. Four reactions used in determining thermodynamic stability: (a) terminal TiOH reacting with I−C_6H_4−CF_3, (b) bridging TiOH reacting with I−C_6H_4−CF_3, (c) terminal TiOH reacting with I−CH_2−C_6H_4−CF_3, and (d) bridging TiOH with I−CH_2−C_6H_4−CF_3.

reaction is set to 0 eV). Reactions with increasingly positive ΔH are less thermodynamically favorable. Thus, the data show that the reaction of I−C_6H_4−CF_3 with the terminal TiOH group (Figure 1a) produces the most thermodynamically favorable binding energy. The second most thermodynamically favorable reaction occurs between I−CH_2−C_6H_4−CF_3 and the terminal TiOH group (Figure 1c). The third most stable reaction is the reaction between the bridging TiOH and I−C_6H_4−CF_3 (Figure 1b), while the least stable reaction involves the bridging TiOH and I−CH_2−C_6H_4−CF_3 (Figure 1d). For both molecules, the reaction occurring at the terminal OH site was ∼0.6−0.7 eV (∼58−67 kJ/mol) more favorable than the reaction occurring at the bridging OH site. The difference between the aryl vs benzyl molecule reacting with the terminal TiOH group is about ∼0.8 eV favoring the aryl molecule, whereas the same two molecules reacting with the bridging TiOH group is about ∼0.3 eV, again favoring the aryl molecule.

Computational Hammett Plots. Hammett plots are widely used to determine the charged state of reaction intermediates in involving aromatic species and can be made on the basis of energy changes (thermodynamic Hammett plot) or reaction rate constants ("kinetic Hammett plot") versus Hammett parameters, σ.[72−76] Electron-withdrawing functional groups yield positive σ values, whereas electron-donating functional groups yield negative σ values. The greater the *absolute* value of σ, the more strongly the functional group influences aromatic ring electron density. The specific case of hydrogen as a functional group is chosen as an arbitrary reference point, so that for this substituent $\sigma = 0$, and the enthalpy of reaction for the H-substituted molecule is used as a reference energy, ΔH_0. Thermodynamic Hammett plots are generally plotted as changes in energy ($\Delta G - \Delta G_0$ or, neglecting entropy effects, $\Delta H - \Delta H_0$) vs σ, while kinetic Hammett plots are plotted as $\ln(k/k_0)$ vs σ, where k *is* the rate

DOI: 10.1021/acs.jpcc.5b08333
J. Phys. Chem. C 2015, 119, 27972−27981

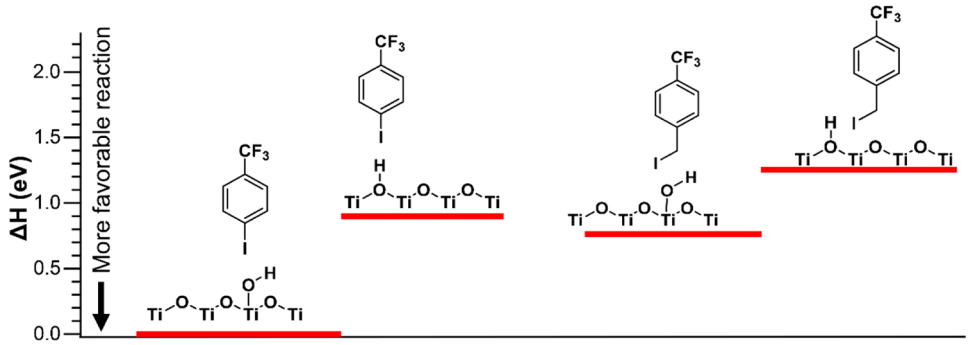

Figure 2. Enthalpies of adsorption for the four reactions shown in Figure 1; in each case it is assumed the indicated reactants form a Ti−O−C surface bond with formation of HI. The enthalpy of reaction for the terminal TiOH group reacting with I−C_6H_4−CF_3 (left-most reaction shown) is set to 0. eV. Positive values of ΔH correspond to less thermodynamically favorable reactions.

constant for reaction with a given substituent group and k_0 is the rate using H as a substituent.

If the rate-limiting step of a reaction is dependent upon substituent effects, then a Hammett plot typically shows a linear trend.[72,73,75,76] The value of the slope, ρ, when the Hammett plot is fit to a line indicates the type of charge being built upon reaction intermediates that incorporate the benzene ring. A negative value of ρ indicates a positive charge is building. Inversely, a positive value of ρ indicates a negative charge is building.[75]

For reactions of the type studied here entropy changes are expected to be very similar for reactions involved different molecules, since in each case the products are HI and a surface-bound molecule with no other significant changes in structure. Consequently, we used our calculated enthalpies to produce our computational Hammett plots, where we have graphed $\Delta H - \Delta H_0$ versus σ for reaction of *para* functionalized iodo aryl species with TiO_2. Table 1 lists the nine functional groups

Table 1. Functional Groups Set *Para* to the Leaving Group in the Iodo Aryl Molecules along with the Corresponding Hammett Parameter (σ) for Each Functional Group

functional group	Hammett parameter, σ	functional group	Hammett parameter, σ
$-NH_2$	−0.66	−F	0.06
−OH	−0.37	−COOH	0.45
$-OCH_3$	−0.27	$-CF_3$	0.54
$-CH_3$	−0.17	$-NO_2$	0.78
−H	0		

studied computationally as well as the corresponding σ value for each group. Because faster reactions are associated with more negative reaction energies, care must be taken regarding sign convention in Hammett plots. For our computational Hammett plots, a *negative* value for ρ indicates *negative* charge building on the reaction intermediate, whereas a *positive* value for ρ indicates *positive* charge building on the reaction intermediate.

Figure 3 shows the computational Hammett plots obtained from when we react the molecules with the terminal TiOH (Figure 3a) and bridging TiOH (Figure 3b) groups. The computational Hammett plots both show a linear trend possessing a positive slope of small (<1) value. The positive slope suggests that positive charge is building throughout the reaction. However, the small absolute values (<1) for the slopes of both plots indicate the substituent groups have relatively

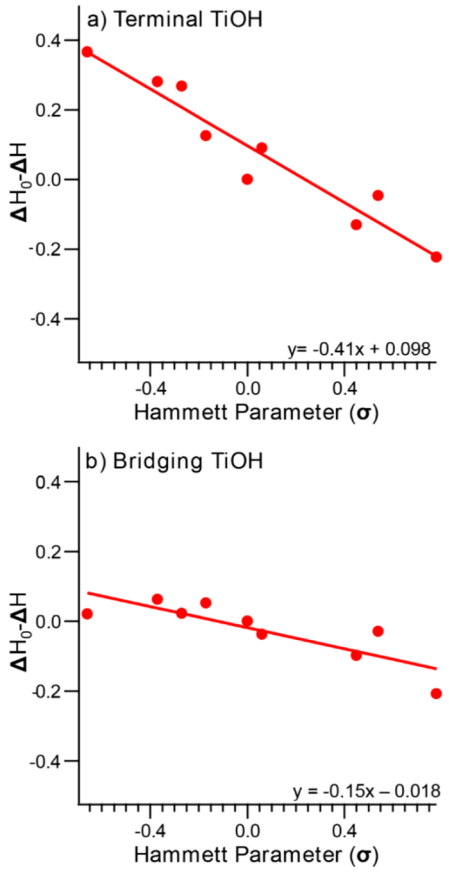

Figure 3. Computational Hammett plots based on calculated enthalpies of adsorption for reactions involving the (a) terminal TiOH and (b) bridging TiOH. Both plots show a slight dependence upon electron-donating groups.

little effect on the thermodynamics and, by extension, with the expected reaction rate. Therefore, in both the terminal and bridging TiOH cases we see that the reaction has a weak dependence upon electron-donating groups that presumably stabilize reaction intermediates.

Experimental Rate Constants and Hammett Plot. Figure 4 shows the first-order rate plots for all five commercially available molecules. To fit these plots, time trials were performed at 65 °C for each molecule. Then, the intensity of characteristic IR vibrations were summed for each molecule, and the total was fit to a first-order kinetic rate law $A_0 = A_{sat}(1 - e^{-kt})$ where A_0 is absorbance at time t, A_{sat} is the maximum

DOI: 10.1021/acs.jpcc.5b08333
J. Phys. Chem. C 2015, 119, 27972−27981

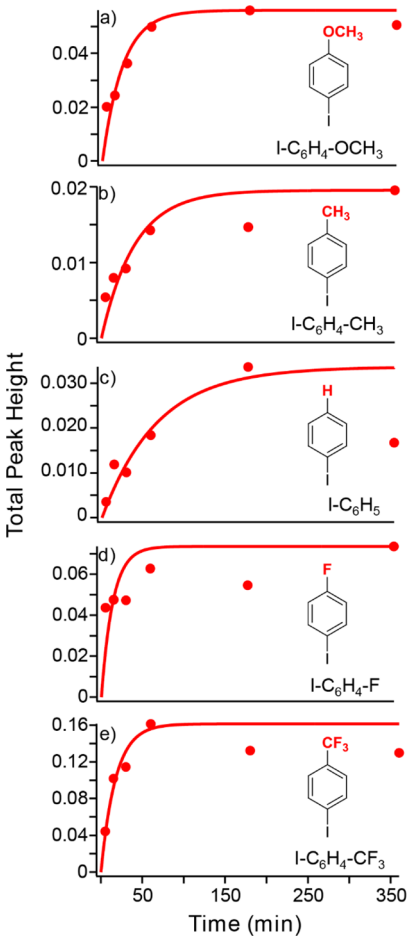

Figure 4. First-order rate constant plots for (a) I−C_6H_4−OCH_3, (b) I−C_6H_4−CH_3, (c) I−C_6H_5, (d) I−C_6H_4−F, and (e) I−C_6H_4−CF_3 reacting with TiO_2 thin films.

absorbance, t is the time in minutes that the reaction vial spent in the oven, and k is the rate constant.

Table 2 shows the k values obtained for each molecule, and the Hammett parameter calculated from these rates. Based on our experiments, I−C_6H_4−F had the fastest reaction rate (4−9 min) out of the five molecules studied, whereas I−C_6H_5 had the slowest reaction rate (45−125 min). Figure 5 shows the experimental Hammett plot. This Hammett plot shows little correlation between the rate of reaction and the σ values. The lack of correlation in a Hammett plot could suggest one of two possibilities: either a change in reaction mechanism is occurring, or the rate-limiting step for the reaction is not dependent upon substituent effects.[74−76]

Table 2. Molecules Used in Making the Experimental Hammett Plot and Rate Constants Obtained from the Langmuir Isotherms (min^{-1})

molecule	Hammett parameter (σ)	rate constant (min^{-1})
I−C_6H_4−OCH_3	−0.27	0.040 ± 0.007
I−C_6H_4−CH_3	−0.17	0.025 ± 0.006
I−C_6H_5	0.00	0.015 ± 0.007
I−C_6H_4−F	0.06	0.18 ± 0.07
I−C_6H_4−CF_3	0.54	0.056 ± 0.014

Determination of Water Solubility Using Quantitative NMR. Zhang et al.[77] studied the reaction of TiO_2 with chlorobenzene and found that the reaction rate depended on the humidity, and on that basis they suggested that the rate of reaction was likely limited by the hydrophilic or hydrophobic nature of the molecules that must travel through the layer of strongly bound water present on TiO_2 surfaces.[77] Since the reactants we use are hydrophobic, we hypothesized that the reaction rates might be limited by diffusion of the reactant through strongly bound water layers. To test this we used NMR experiments to assess the solubility of each molecule in water. Using sodium-3-(trimethylsilyl)-1-propanesulfonic acid as an internal standard, we mixed our prepared internal standard solutions in D_2O solvent with an excess of each molecule and placed each reaction vial into a 65 °C oven. After leaving the vials in the oven for time scales longer than the inverse reaction rates, we performed NMR and quantified the amounts of molecule detected. Figure 6 shows the resulting solubility trend from our measurements. In Figure 6, we see that I−C_6H_5 is the most soluble (0.9 mM), followed by I−C_6H_4−OCH_3 and I−C_6H_4−F (0.8 mM, each), then I−C_6H_4−CH_3 (0.4 mM), and finally I−C_6H_4−CF_3 (0.2 mM). This trend does not explain the results seen in our experimental Hammett plot based on rates of reaction. Indeed, the molecule with the slowest reaction rate, I−C_6H_5, appears to be one of the most water-soluble.

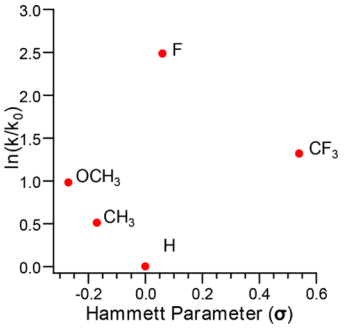

Figure 5. Experimental Hammett plot based on rate constants. No dependence upon substituent effects is apparent.

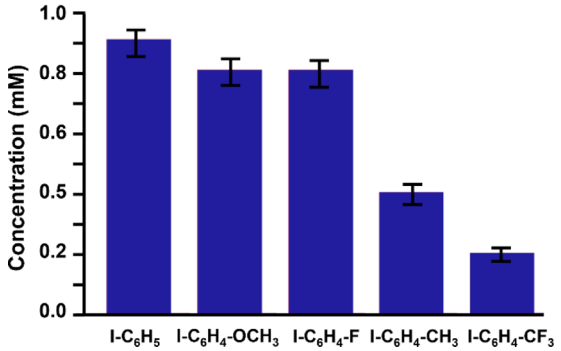

Figure 6. NMR solubility comparison for the five molecules studied experimentally.

Monitoring Loss of Water as Reaction Progresses. Mass spectrometry results indicate the rate of water loss through the *in situ* monitoring of the reactions between TiO_2 and I−C_6H_5 and I−C_6H_4−CF_3. I−C_6H_5 has the slowest reaction rate based on FTIR results but is one of the most water-soluble molecules based on NMR results. Likewise, I−C_6H_4−CF_3 reacts much faster but is the least water-soluble molecule. Therefore, monitoring the loss of water (m/z = 18) for the reactions between TiO_2 and these two molecules

DOI: 10.1021/acs.jpcc.5b08333
J. Phys. Chem. C 2015, 119, 27972−27981

provides insight into how the water layer affects the rate of reaction.

Figure 7 shows a plot of m/z = 18 peak height (from desorbing water) vs time for the reactions run for 3 is the

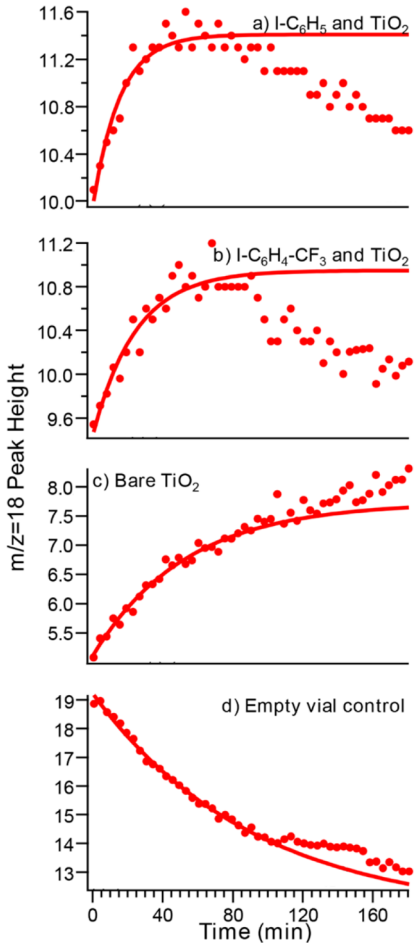

Figure 7. Height of m/z = 18 mass spectrometry peak vs time. Mass spectrometry data were collected at 65 °C for a total of 3 h for (a) I–C_6H_5 reacting with TiO_2, (b) I–C_6H_4–CF_3 reacting with TiO_2, (c) bare TiO_2, and (d) an empty reaction vial.

reaction time, x_0 is the reaction start time (0 min), and τ is decay constant, we obtain values for τ of 15 and 24 min for I–C_6H_5 and I–C_6H_4–CF_3, respectively. Based on these values, water leaves about 9 min faster during the reaction between TiO_2 and I–C_6H_5 than for the reaction between TiO_2 and I–C_6H_4–CF_3. Both these τ values are faster than the bare TiO_2 (Figure 7c) or empty reaction vial (Figure 7d) controls performed.

DISCUSSION

The goal of this study was to determine what effects substituents have on the thermal grafting of aromatic molecules to TiO_2 surfaces. The arenes used in this study were chosen because they are commercially available and possessed a wide range of chemical functionality. These small aromatic molecules also served as model systems for larger, less conveniently attainable, molecular sensitizers and photocatalysts. The results of our studies indicate that a simple, straightforward interpretation is not possible.

First, we will discuss the results of the aryl versus benzyl bond stability comparison. Based on the calculations performed, the aryl molecule–surface attachment is thermodynamically more stable than the benzyl molecule–surface attachment. There are also two possible TiOH groups on the surface,[78,79] and consequently there are two possible types of surface sites that could participate in this thermal grafting reaction. Comparing the bridging and terminal TiOH groups, the terminal TiOH resulted in more stable bonds forming between the molecule and the surface. However, prior work showing 4-iodomethyl-TFMB also reacting with the surface[13] indicates that the $\Delta(\Delta G)$ between the most thermodynamically stable and the least thermodynamically stable reaction of about 1.5 eV (~144 kJ/mol) is not a large enough barrier to prevent any of the reactions studied from occurring. Therefore, there is the possibility that both TiOH groups may react with the molecule(s). The significance in this statement is that the amount of surface sites able to participate will affect both the overall reaction and the resulting surface coverage.

The NBO analysis may provide some insight into the thermodynamic stability trends we see. In the case where the aryl molecules react with the terminal TiOH group, the oxygen atom actually has two interactions with the carbon atom on the molecule. For the other three cases shown in Figure 1, the oxygen only has one interaction with the carbon atom on the molecule. In all cases, the bonds formed were polarized with about 70% of the electron density on the oxygen and 30% on the carbon. Because of these findings, we speculate that since the oxygen in the terminal TiOH is above the TiO_2 surface plane while the oxygen in the bridging TiOH is part of the TiO_2 surface an effect on the oxygen–carbon interactions may be felt; for the terminal TiOH, there are no other atoms as nearest neighbors, whereas for the bridging TiOH there are nearest neighbors. With no neighbors, the oxygen in the terminal TiOH is able to form more interactions with the molecule. For the bridging TiOH, however, the oxygen is part of the surface and participates in the TiO_2 electronic structure. Consequently, the oxygen in the bridging TiOH is less free to electronically interact with the molecule.

Our computational and experimental Hammett plots disagreed. The reason behind this is most likely due to the absence of an experimental parameter in the computational modeling. Specifically, the TiO_2 surface is very hydrophilic and can be covered by multilayers of adsorbed and dissociated water. To include such a complex factor in the computations would have greatly increased the computational cost for little payoff. However, combining the absence of the water layer in the computations with the discrepancy seen between the computational and experimental Hammett plots suggests that the water layer may be behind the trend in reactivity we see experimentally.

There is evidence in the literature to support that the water layer can affect interactions at the molecule–TiO_2 interface. Zhang and co-workers[77] noticed that the photodegradation of different molecules did not appear to follow a trend in relation to rates of photodegradation and set about looking at the effects of humidity on the adsorption of chlorobenzene on TiO_2. To study the effects of humidity, Zhang and co-workers[77] performed experiments where they would introduce a constant concentration of chlorobenzene into a reaction vessel coated with TiO_2 similar to our mass spectrometry reaction vials and then vary the amount of humidity introduced. They found a direct correlation between amount of humidity present in the

DOI: 10.1021/acs.jpcc.5b08333
J. Phys. Chem. C 2015, 119, 27972–27981

vial and the amount of chlorobenzene degraded. This finding is significant for our work, as it serves as an indication that the water layer present on the TiO_2 surface does affect the ability of a molecule to reach the TiO_2–water interface.

Most studies of the water layer on the TiO_2 surface have been computational[61−67] or UHV[78−83] in nature. The work done by Zhang et al.[77] is one of the few studies that relates most closely to benchtop chemistry. We aim to add to the body of benchtop-chemistry evidence through investigating the effects of the presence of water on the thermal grafting reaction. To start probing the effects of the water layer, we first determined the water solubility of the molecules. Using variable temperature NMR to measure the presence of organic compound present in D_2O at 65 °C, we determined the following trend, from most to least water-soluble:

$$I{-}C_6H_5 > I{-}C_6H_4{-}OCH_3 \approx I{-}C_6H_4{-}F > I{-}C_6H_4{-}CH_3 > I{-}C_6H_4{-}CF_3$$

These NMR results did not correlate with the experimental Hammett plot. Therefore, we next set up the *in situ* mass spectrometry experiments to monitor for loss of the H_2O layer on the TiO_2 surface as the reaction progresses.

For the mass spectrometry experiments, we monitored for the loss of the H_2O layer on the TiO_2 surface. Using mass spectrometry, we were able to determine time dependence of the water loss. We looked at $I{-}C_6H_5$ and $I{-}C_6H_4{-}CF_3$ for these experiments, as these molecules were the most and least water-soluble, respectively, while also possessing reaction rate constants very different from each other. What we found was that the $I{-}C_6H_5$ resulted in faster water loss based on the time-dependent data. These mass spectrometry findings agree with our NMR results.

Neither the NMR nor mass spectrometry results agree with the hypothesis of Zhang et al.[77] that molecular hydrophilicity affects the rate of reaction. Our work cannot be directly compared to theirs, however. First, Zhang and co-workers only studied the effects of humidity on one molecule, whereas we studied the effects of humidity on five molecules; our findings incorporate a broader molecular basis for our comparison. Second, Zhang et al.[77] were studying the effects of humidity on the photodegradation of chlorobenzene. Most likely, the mechanism of photodegradation is not the same as the mechanism for thermal grafting. For one, generally photodegradation occurs through ·OH radical formation,[77,84−88] and water is needed for ·OH radical formation. If the water is driven off during thermal grafting, as seen in our mass spectrometry, then there is no source for ·OH radicals. Instead, the aromatic molecules only need come into contact with radicals that would also be in the water layer. In this way, photodegradation is like the solution-based reactions in organic chemistry. For surface functionalization to occur, however, the molecule must come into contact with the surface so that a molecule–surface bond may form. Therefore, thermal grafting is inherently different from photodegradation, and through association so are the effects the water layer has on the extent of reaction.

CONCLUSIONS

We have shown that thermal grafting supports a wide scope of molecules that will form new bonds to the TiO_2 surface. Our results indicate that the rates of reaction between different molecules are not easily understood on the basis of simple chemical principles such as inductive effect, nor is there a clear correlation between the hydrophobic character and its reactivity under benchtop conditions. This in turn suggests that surface water layers on TiO_2 are unlikely to control the overall reaction rate. Further studies probing various radical-based pathways may provide additional insights into these reactions. The qualitative information provided here will provide guidance for further work tethering complex, functional molecules to TiO_2 surfaces.

ASSOCIATED CONTENT

Supporting Information

The Supporting Information is available free of charge on the ACS Publications website at DOI: 10.1021/acs.jpcc.5b08333.

Nuclear magnetic resonance (NMR) temperature calibration; determination of T_1 relaxation time; NMR spectra from water solubility experiments; sample FTIR spectra and spectral ranges used in analysis (PDF)

AUTHOR INFORMATION

Corresponding Author

*E-mail: rjhamers@wisc.edu (R.J.H.).

Notes

The authors declare no competing financial interest.

ACKNOWLEDGMENTS

This work was supported by the National Science Foundation grant CHE-1310293. The authors thank Benjamin D. Dunnington and J. R. Schmidt for their help with understanding VASP and for their NBO analysis code for VASP outputs, Joseph C. Yeager and Kacie M. Louis for their help in starting VASP calculations, Charlie Fry for his help in performing the temperature-dependent NMR, Christopher S. Adams for his help in discussing organic chemistry analogies to thermal grafting, and Marco D. Torelli and Madeleine M. Meyer for the anatase TiO_2 nanoparticles for the mass spectrometry experiments.

REFERENCES

(1) O'Regan, B.; Gratzel, M. A Low-Cost, High-Efficiency Solar Cell Based on Dye-Sensitized Colloidal TiO_2 Films. *Nature* **1991**, *353*, 737−740.

(2) Kroeze, J. E.; Hirata, N.; Koops, S.; Nazeeruddin, M. K.; Schmidt-Mende, L.; Gratzel, M.; Durrant, J. R. Alkyl Chain Barriers for Kinetic Optimization in Dye-Sensitized Solar Cells. *J. Am. Chem. Soc.* **2006**, *128*, 16376−16383.

(3) Hagberg, D. P.; Yum, J. H.; Lee, H.; De Angelis, F.; Marinado, T.; Karlsson, K. M.; Humphry-Baker, R.; Sun, L. C.; Hagfeldt, A.; Gratzel, M.; et al. Molecular Engineering of Organic Sensitizers for Dye-Sensitized Solar Cell Applications. *J. Am. Chem. Soc.* **2008**, *130*, 6259−6266.

(4) Li, C. H.; Wang, F.; Yu, J. C. Semiconductor/Biomolecular Composites for Solar Energy Applications. *Energy Environ. Sci.* **2011**, *4*, 100−113.

(5) Mulhern, K. R.; Detty, M. R.; Watson, D. F. Effects of Surface-Anchoring Mode and Aggregation State on Electron Injection from Chalcogenorhodamine Dyes to Titanium Dioxide. *J. Photochem. Photobiol., A* **2013**, *264*, 18−25.

(6) Unger, E. L.; Edvinsson, T.; Roy-Mayhew, J. D.; Rensmo, H.; Hagfeldt, A.; Johansson, E. M. J.; Boschloo, G. Excitation Energy Dependent Charge Separation at Hole-Transporting Dye/TiO_2 Hetero Interface. *J. Phys. Chem. C* **2012**, *116*, 21148−21156.

(7) Campbell, W. M.; Burrell, A. K.; Officer, D. L.; Jolley, K. W. Porphyrins as Light Harvesters in the Dye-Sensitised TiO_2 Solar Cell. *Coord. Chem. Rev.* **2004**, *248*, 1363−1379.

DOI: 10.1021/acs.jpcc.5b08333
J. Phys. Chem. C 2015, 119, 27972−27981

(8) Kohtani, S.; Nishioka, S.; Yoshioka, E.; Miyabe, H. Dye-Sensitized Photo-Hydrogenation of Aromatic Ketones on Titanium Dioxide under Visible Light Irradiation. *Catal. Commun.* **2014**, *43*, 61−65.
(9) Cherevatskaya, M.; Neumann, M.; Fuldner, S.; Harlander, C.; Kummel, S.; Dankesreiter, S.; Pfitzner, A.; Zeitler, K.; Konig, B. Visible-Light-Promoted Stereoselective Alkylation by Combining Heterogeneous Photocatalysis with Organocatalysis. *Angew. Chem., Int. Ed.* **2012**, *51*, 4062−4066.
(10) Yuan, Y. J.; Yu, Z. T.; Zhang, J. Y.; Zou, Z. G. A Copper(I) Dye-Sensitised TiO_2-Based System for Efficient Light Harvesting and Photoconversion of CO_2 into Hydrocarbon Fuel. *Dalton Trans.* **2012**, *41*, 9594−9597.
(11) Galoppini, E. Linkers for Anchoring Sensitizers to Semiconductor Nanoparticles. *Coord. Chem. Rev.* **2004**, *248*, 1283−1297.
(12) Galoppini, E.; Guo, W. Z.; Zhang, W.; Hoertz, P. G.; Qu, P.; Meyer, G. J. Long-Range Electron Transfer Across Molecule-Nanocrystalline Semiconductor Interfaces using Tripodal Sensitizers. *J. Am. Chem. Soc.* **2002**, *124*, 7801−7811.
(13) English, C. R.; Bishop, L. M.; Chen, J. X.; Hamers, R. J. Formation of Self-Assembled Monolayers of π-Conjugated Molecules on TiO_2 Surfaces by Thermal Grafting of Aryl and Benzyl Halides. *Langmuir* **2012**, *28*, 6866−6876.
(14) Bishop, L. M.; Yeager, J. C.; Chen, X.; Wheeler, J. N.; Torelli, M. D.; Benson, M. C.; Burke, S. D.; Pedersen, J. A.; Hamers, R. J. A Citric Acid-Derived Ligand for Modular Functionalization of Metal Oxide Surfaces via "Click" Chemistry. *Langmuir* **2012**, *28*, 1322−1329.
(15) Hirva, P.; Haukka, M. Effect of Different Anchoring Groups on the Adsorption of Photoactive Compounds on the Anatase (101) Surface. *Langmuir* **2010**, *26*, 17075−17081.
(16) Brown, D. G.; Schauer, P. A.; Borau-Garcia, J.; Fancy, B. R.; Berlinguette, C. P. Stabilization of Ruthenium Sensitizers to TiO_2 Surfaces through Cooperative Anchoring Groups. *J. Am. Chem. Soc.* **2013**, *135*, 1692−1695.
(17) Brennan, B. J.; Portoles, M. J. L.; Liddell, P. A.; Moore, T. A.; Moore, A. L.; Gust, D. Comparison of Silatrane, Phosphonic Acid, and Carboxylic Acid Functional Groups for Attachment of Porphyrin Sensitizers to TiO_2 in Photoelectrochemical Cells. *Phys. Chem. Chem. Phys.* **2013**, *15*, 16605−16614.
(18) Cui, J.; Lu, J.; Xu, X.; Cao, K.; Wang, Z.; Alemu, G.; Yuang, H.; Shen, Y.; Xu, J.; Cheng, Y.; et al. Organic Sensitizers with Pyridine Ring Anchoring Group for p-Type Dye-Sensitized Solar Cells. *J. Phys. Chem. C* **2014**, *118*, 16433−16440.
(19) Hagfeldt, A.; Boschloo, G.; Sun, L. C.; Kloo, L.; Pettersson, H. Dye-Sensitized Solar Cells. *Chem. Rev.* **2010**, *110*, 6595−6663.
(20) Ronca, E.; Pastore, M.; Belpassi, L.; Tarantelli, F.; De Angelis, F. Influence of the Dye Molecular Structure on the TiO_2 Conduction Band in Dye-Sensitized Solar Cells: Disentangling Charge Transfer and Electrostatic Effects. *Energy Environ. Sci.* **2013**, *6*, 183−193.
(21) Wang, X.; Guo, L.; Xia, P. F.; Zheng, F.; Wong, M. S.; Zhu, Z. Effects of Surface Modification on Dye-Sensitized Solar Cell Based on an Organic Dye with Naphtho[2,1-b:3,4-b′]dithiophene as the Conjugated Linker. *ACS Appl. Mater. Interfaces* **2014**, *6*, 1926−1932.
(22) Roelofs, K. E.; Brennan, T. P.; Bent, S. F. Interface Engineering in Inorganic-Absorber Nanostructured Solar Cells. *J. Phys. Chem. Lett.* **2014**, *5*, 348−360.
(23) Sewvandi, G. A.; Tao, Z.; Kusunose, T.; Tanaka, Y.; Nakanishi, S.; Feng, Q. Modification of TiO_2 Electrode with Organic Silane Interposed Layer for High-Performance of Dye-Sensitized Solar Cells. *ACS Appl. Mater. Interfaces* **2014**, *6*, 5818−5826.
(24) An, H.; Song, D.; Lee, J.; Kang, E. M.; Jaworski, J.; Kim, J. M.; Kang, Y. S. Promotion of Strongly Anchored Dyes on the Surface of Titania by Tetraethyl Orthosilicate Treatment for Enhanced Solar Cell Performance. *J. Mater. Chem. A* **2014**, *2*, 2250−2255.
(25) Sanchez-de-Armas, R.; Oviedo, J.; Miguel, M. A. S.; Sanz, J. F. Direct vs Indirect Mechanisms for Electron Injection in Dye-Sensitized Solar Cells. *J. Phys. Chem. C* **2011**, *115*, 11293−11301.
(26) Ganesan, P.; Chandiran, A.; Gao, P.; Rajalingam, R.; Grätzel, M.; Nazeeruddin, M. K. Molecular Engineering of 2-Quinolinone Based Anchoring Groups for Dye-Sensitized Solar Cells. *J. Phys. Chem. C* **2014**, *118*, 16896−16903.
(27) Yang, J.; Ganesan, P.; Teuscher, J.; Moehl, T.; Kim, Y. J.; Yi, C.; Comte, P.; Pei, K.; Holcombe, T. W.; Nazeeruddin, M. K.; et al. Influence of the Donor Size in D−π−A Organic Dyes for Dye-Sensitized Solar Cells. *J. Am. Chem. Soc.* **2014**, *136*, 5722−5730.
(28) Wang, X. F.; Tamiaki, H.; Kitao, O.; Ikeuchi, T.; Sasaki, S. Molecular Engineering on a Chlorophyll Derivative, Chlorin e(6), for Significantly Improved Power Conversion Efficiency in Dye-Sensitized Solar Cells. *J. Power Sources* **2013**, *242*, 860−864.
(29) Grisorio, R.; De Marco, L.; Allegretta, G.; Giannuzzi, R.; Suranna, G. P.; Manca, M.; Mastrorilli, P.; Gigli, G. Anchoring Stability and Photovoltaic Properties of New D(-π-A)$_2$ Dyes for Dye-Sensitized Solar Cell Applications. *Dyes Pigm.* **2013**, *98*, 221−231.
(30) Iqbal, Z.; Wu, W.-Q.; Zhang, H.; Hua, P.-L.; Fang, X.; Kuang, D.-B.; Wang, L.; Meier, H.; Cao, D. Impact of Hydroxy and Octyloxy Substituents of Phenothiazine Based Dyes on the Photovoltaic Performance. *Dyes Pigm.* **2013**, *99*, 299−307.
(31) Feng, Q. Y.; Zhou, G.; Wang, Z. S. Varied Alkyl Chain Functionalized Organic Dyes for Efficient Dye-Sensitized Solar Cells: Influence of Alkyl Substituent Type on Photovoltaic Properties. *J. Power Sources* **2013**, *239*, 16−23.
(32) Zhang, J.; Kan, Y. H.; Li, H. B.; Geng, Y.; Wu, Y.; Su, Z. M. How to Design Proper π-spacer Order of the D-π-A dyes for DSSCs? A Density Functional Response. *Dyes Pigm.* **2012**, *95*, 313−321.
(33) Mathew, S.; Yella, A.; Gao, P.; Humphry-Baker, R.; Curchod, B. F. E.; Ashari-Astani, N.; Tavernelli, I.; Rothlisberger, U.; Nazeeruddin, M. K.; Grätzel, M. Dye-sensitized Solar Cells with 13% Efficiency Achieved through the Molecular Engineering of Porphyrin Sensitizers. *Nat. Chem.* **2014**, *6*, 242−247.
(34) Wang, Z.; Liang, M.; Wang, H.; Wang, P.; Cheng, F.; Sun, Z.; Song, X. Joint Electrical, Photophysical, and Photovoltaic Studies on Truxene Dye-Sensitized Solar Cells: Impact of Arylamine Electron Donors. *ChemSusChem* **2014**, *7*, 795−803.
(35) Venkateswararao, A.; Thomas, K. R. J.; Lee, C. P.; Li, C. T.; Ho, K. C. Organic Dyes Containing Carbazole as Donor and π-Linker: Optical, Electrochemical, and Photovoltaic Properties. *ACS Appl. Mater. Interfaces* **2014**, *6*, 2528−2539.
(36) Murakami, T. N.; Koumura, N.; Kimura, M.; Mori, S. Structural Effect of Donor in Organic Dye on Recombination in Dye-Sensitized Solar Cells with Cobalt Complex Electrolyte. *Langmuir* **2014**, *30* (8), 2274−2279.
(37) Mao, J.; Yang, J.; Teuscher, J.; Moehl, T.; Yi, C.; Humphry-Baker, R.; Comte, P.; Grätzel, C.; Hua, J.; Zakeeruddin, S. M.; Tian, H.; Grätzel, M. Thiadiazolo[3,4-*c*]pyridine Acceptor Based Blue Sensitizers for High Efficiency Dye-Sensitized Solar Cells. *J. Phys. Chem. C* **2014**, *118*, 17090−17099.
(38) Wu, G.; Kong, F.; Zhang, Y.; Zhang, X.; Li, J.; Chen, W.; Liu, W.; Ding, Y.; Zhang, C.; Zhang, B.; Yao, J.; Dai, S. Multiple-Anchoring Triphenylamine Dyes for Dye-Sensitized Solar Cell Application. *J. Phys. Chem. C* **2014**, *118*, 8756−8765.
(39) Bagno, A.; Scorrano, G.; Terrier, F. Kinetics of Nucleophilic Aromatic Substitution in Concentrated Solutions of Alkali Metal Methoxides in Methanol. *J. Chem. Soc., Perkin Trans. 2* **1991**, *5*, 651−655.
(40) Crampton, M. R.; Emokpae, T. A.; Isanbor, C. The Effects of Ring Substituents and Leaving Groups on the Kinetics of SNAr Reactions of 1-Halogeno- and 1-Phenoxy-nitrobenzenes with Aliphatic Amines in Acetonitrile. *Eur. J. Org. Chem.* **2007**, *2007* (8), 1378−1383.
(41) Strauss, M. J. Anionic Sigma Complexes. *Chem. Rev.* **1970**, *70* (6), 667−712.
(42) Burnett, J. F.; Zahler, R. E. Aromatic Nucleophilic Substitution Reactions. *Chem. Rev.* **1951**, *49*, 273−412.
(43) Fyfe, C. A.; Damji, S. W. H.; Koll, A. Low-Temperature Flow NMR Investigation of the Transient Intermediate in the Nucleophilic Aromatic Substitution of 2,4,6-Trinitroanisole by n-Butylamine. *J. Am. Chem. Soc.* **1979**, *101*, 951−955.

DOI: 10.1021/acs.jpcc.5b08333
J. Phys. Chem. C 2015, 119, 27972−27981

(44) Ooyama, Y.; Harima, Y. Molecular Designs and Syntheses of Organic Dyes for Dye-Sensitized Solar Cells. *Eur. J. Org. Chem.* **2009**, *2009*, 2903−2934.
(45) Siva Kumar, G.; Srinivas, K.; Shanigaram, B.; Bharath, D.; Singh, S. P.; Bhanuprakash, K.; Rao, V. J.; Islam, A.; Han, L. Metal-Free Organic Dyes Containing Thiadiazole Unit for Dye-Sensitized Solar Cells: A Combined Experimental and Theoretical Study. *RSC Adv.* **2014**, *4*, 13172−13181.
(46) Maeda, T.; Nitta, S.; Nakao, H.; Yagi, S.; Nakazumi, H. Squaraine Dyes with Pyrylium and Thiopyrylium Components for Harvest of Near Infrared Light in Dye-Sensitized Solar Cells. *J. Phys. Chem. C* **2014**, *118*, 16618−16625.
(47) Tan, L.-l.; Huang, J.-F.; Shen, Y.; Xiao, L.-M.; Liu, J.; Kuang, D.-B.; Su, C.-Y. Highly Efficient and Stable Organic Sensitizers with Duplex Starburst Triphenylamine and Carbazole Donors for Liquid and Quasi-solid-state Dye-sensitized Solar Cells. *J. Mater. Chem. A* **2014**, *2*, 8988−8994.
(48) Asbury, J. B.; Hao, E.; Wang, Y. Q.; Ghosh, H. N.; Lian, T. Q. Ultrafast Electron Transfer Dynamics from Molecular Adsorbates to Semiconductor Nanocrystalline Thin Films. *J. Phys. Chem. B* **2001**, *105*, 4545−4557.
(49) Asbury, J. B.; Hao, E. C.; Wang, Y. Q.; Lian, T. Q. Bridge Length-Dependent Ultrafast Electron Transfer from Re Polypyridyl Complexes to Nanocrystalline TiO_2 Thin Films Studied by Femtosecond Infrared Spectroscopy. *J. Phys. Chem. B* **2000**, *104*, 11957−11964.
(50) Paoprasert, P.; Laaser, J. E.; Xiong, W.; Franking, R. A.; Hamers, R. J.; Zanni, M. T.; Schmidt, J. R.; Gopalan, P. Bridge-Dependent Interfacial Electron Transfer from Rhenium-Bipyridine Complexes to TiO_2 Nanocrystalline Thin Films. *J. Phys. Chem. C* **2010**, *114*, 9898−9907.
(51) Chen, J.; Ruther, R. E.; Tan, Y.; Bishop, L. M.; Hamers, R. J. Molecular Adsorption on ZnO($10\bar{1}0$) Single-Crystal Surfaces: Morphology and Charge Transfer. *Langmuir* **2012**, *28*, 10437−10445.
(52) Kotsokechagia, T.; Cellesi, F.; Thomas, A.; Niederberger, M.; Tirelli, N. Preparation of Ligand-Free TiO_2 (Anatase) Nanoparticles through a Nonaqueous Process and Their Surface Functionalization. *Langmuir* **2008**, *24*, 6988−6997.
(53) Kresse, G.; Furthmuller, J. Efficient Iterative Schemes for Ab-Initio Total-Energy Calculations Using a Plane-Wave Basis Set. *Phys. Rev. B: Condens. Matter Mater. Phys.* **1996**, *54*, 11169−11186.
(54) Kresse, G.; Furthmuller, J. Efficiency of Ab-Initio Total Energy Calculations for Metals and Semiconductors Using a Plane-Wave Basis Set. *Comput. Mater. Sci.* **1996**, *6*, 15−50.
(55) Kresse, G.; Hafner, J. Ab-Initio Molecular-Dynamics Simulation of the Liquid-Metal Amorphous-Semiconductor Transition in Germanium. *Phys. Rev. B: Condens. Matter Mater. Phys.* **1994**, *49*, 14251−14269.
(56) Kresse, G.; Hafner, J. Ab-Initio Molecular-Dynamics for Liquid-Metals. *Phys. Rev. B: Condens. Matter Mater. Phys.* **1993**, *47*, 558−561.
(57) Blochl, P. E. Projector Augmented-Wave Method. *Phys. Rev. B: Condens. Matter Mater. Phys.* **1994**, *50*, 17953−17979.
(58) Kresse, G.; Joubert, D. From Ultrasoft Pseudopotentials to the Projector Augmented-Wave Method. *Phys. Rev. B: Condens. Matter Mater. Phys.* **1999**, *59*, 1758−1775.
(59) Perdew, J. P.; Burke, K.; Ernzerhof, M. Generalized Gradient Approximation Made Simple (vol 77, pg 3865, 1996). *Phys. Rev. Lett.* **1997**, *78*, 1396−1396.
(60) Perdew, J. P.; Burke, K.; Ernzerhof, M. Generalized Gradient Approximation Made Simple. *Phys. Rev. Lett.* **1996**, *77*, 3865−3868.
(61) Vittadini, A.; Selloni, A.; Rotzinger, F. P.; Grätzel, M. Structure and Energetics of Water Adsorbed at TiO_2 Anatase (101) and (001) Surfaces. *Phys. Rev. Lett.* **1998**, *81*, 2954−2957.
(62) Liu, S. W.; Yu, J. G.; Jaroniec, M. Anatase TiO_2 with Dominant High-Energy {001} Facets: Synthesis, Properties, and Applications. *Chem. Mater.* **2011**, *23*, 4085−4093.
(63) Bredow, T.; Jug, K. Theoretical Investigation of Water-Adsorption at Rutile and Anatase Surfaces. *Surf. Sci.* **1995**, *327*, 398−408.
(64) Calatayud, M.; Minot, C. Effect of Relaxation on Structure and Reactivity of Anatase (1 0 0) and (0 0 1) Surfaces. *Surf. Sci.* **2004**, *552*, 169−179.
(65) Sumita, M.; Hu, C. P.; Tateyama, Y. Interface Water on TiO_2 Anatase (101) and (001) Surfaces: First-Principles Study with TiO_2 Slabs Dipped in Bulk Water. *J. Phys. Chem. C* **2010**, *114*, 18529−18537.
(66) Vittadini, A.; Casarin, M.; Selloni, A. Chemistry of and on TiO_2-Anatase Surfaces by DFT Calculations: a Partial Review. *Theor. Chem. Acc.* **2007**, *117*, 663−671.
(67) Sun, C. H.; Liu, L. M.; Selloni, A.; Lu, G. Q.; Smith, S. C. Titania-Water Interactions: A Review of Theoretical Studies. *J. Mater. Chem.* **2010**, *20*, 10319−10334.
(68) Chen, J.; Franking, R.; Ruther, R. E.; Tan, Y.; He, X.; Hogendoorn, S. R.; Hamers, R. J. Formation of Molecular Monolayers on TiO_2 Surfaces: A Surface Analogue of the Williamson Ether Synthesis. *Langmuir* **2011**, *27*, 6879−6889.
(69) Williamson, A. Theory of Aetherification. *Philos. Mag.* **1850**, *37*, 350−356.
(70) Monkhorst, H. J.; Pack, J. D. Special Points for Brillouin-Zone Integrations. *Phys. Rev. B* **1976**, *13*, 5188−5192.
(71) Dunnington, B. D.; Schmidt, J. R. Generalization of Natural Bond Orbital Analysis to Periodic Systems: Applications to Solids and Surfaces via Plane-Wave Density Functional Theory. *J. Chem. Theory Comput.* **2012**, *8*, 1902−1911.
(72) Hammett, L. P. The Effect of Structure upon the Reactions of Organic Compounds. Benzene Derivatives. *J. Am. Chem. Soc.* **1937**, *59*, 96−103.
(73) Hansch, C.; Leo, A.; Taft, R. W. A Survey of Hammett Substituent Constants and Resonance and Field Parameters. *Chem. Rev.* **1991**, *91*, 165−195.
(74) Hansch, C.; Leo, A. *Exploring QSAR: Fundamentals and Applications in Chemistry and Biology*; American Chemical Society: Washington, DC, 1995; Vol. *1*.
(75) Anslyn, E. V.; Dougherty, D. A. *Modern Physical Organic Chemistry*; University Science Books: Sausalito, CA, 2006.
(76) Hammett, L. P. Some Relations between Reaction Rates and Equilibrium Constants. *Chem. Rev.* **1935**, *17*, 125−136.
(77) Zhang, L. F.; Anderson, W. A.; Sawell, S.; Moralejo, C. Mechanistic Analysis on the Influence of Humidity on Photocatalytic Decomposition of Gas-Phase Chlorobenzene. *Chemosphere* **2007**, *68*, 546−553.
(78) Gamble, L.; Jung, L. S.; Campbell, C. T. Decomposition and Protonation of Surface Ethoxys on TiO_2(110). *Surf. Sci.* **1996**, *348*, 1−16.
(79) Henderson, M. A. Structural Sensitivity in the Dissociation of Water on TiO_2 Single-Crystal Surfaces. *Langmuir* **1996**, *12*, 5093−5098.
(80) Soria, J.; Sanz, J.; Sobrados, I.; Coronado, J. M.; Maira, A. J.; Hernandez-Alonso, M. D.; Fresno, F. FTIR and NMR Study of the Adsorbed Water on Nanocrystalline Anatase. *J. Phys. Chem. C* **2007**, *111*, 10590−10596.
(81) Herman, G. S.; Dohnalek, Z.; Ruzycki, N.; Diebold, U. Experimental investigation of the interaction of water and methanol with anatase-TiO_2(101). *J. Phys. Chem. B* **2003**, *107*, 2788−2795.
(82) Zhang, Z.; Bondarchuk, O.; Kay, B. D.; White, J. M.; Dohnalek, Z. Imaging Water Dissociation on TiO_2(110): Evidence for Inequivalent Geminate OH Groups. *J. Phys. Chem. B* **2006**, *110*, 21840−21845.
(83) Hugenschmidt, M. B.; Gamble, L.; Campbell, C. T. The Interaction of H_2O with a TiO_2(110) Surface. *Surf. Sci.* **1994**, *302*, 329−340.
(84) Lee, S. Y.; Park, S. J. TiO_2 Photocatalyst for Water Treatment Applications. *J. Ind. Eng. Chem.* **2013**, *19*, 1761−1769.
(85) Okamoto, K.; Yamamoto, Y.; Tanaka, H.; Itaya, A. Kinetics of Heterogenous Photocatalytic Decomposition of Phenol over Anatase TiO_2 Powder. *Bull. Chem. Soc. Jpn.* **1985**, *58*, 2023−2028.

DOI: 10.1021/acs.jpcc.5b08333
J. Phys. Chem. C 2015, 119, 27972−27981

(86) Okamoto, K.; Yamamoto, Y.; Tanaka, H.; Tanaka, M.; Itaya, A. Heterogenous Photocatalytic Decomposition of Phenol over TiO_2 Powder. *Bull. Chem. Soc. Jpn.* **1985**, *58*, 2015−2022.
(87) Izumi, I.; Dunn, W. W.; Wilbourn, K. O.; Fan, F. R. F.; Bard, A. J. Heterogenous Photocatalytic Oxidation of Hydrocarbons on Platinized TiO_2 Powders. *J. Phys. Chem.* **1980**, *84*, 3207−3210.
(88) Izumi, I.; Fan, F. R. F.; Bard, A. J. Heterogenous Photocatalytic Decomposition of Benzoic Acid and Adipic Acid on Platinized TiO_2 Powder - The Phot-Kolbe Decarboxylative Route to the Breakdown on the Benzene Ring and to the Production of Butane. *J. Phys. Chem.* **1981**, *85*, 218−223.

DOI: 10.1021/acs.jpcc.5b08333
J. Phys. Chem. C 2015, 119, 27972−27981